# Vascular 3D+T Freehand Ultrasound Using Correlation of Doppler and Pulse-Oximetry Data

Christoph Hennersperger, Athanasios Karamalis, and Nassir Navab

Chair for Computer Aided Medical Procedures (CAMP), TU Munich, Germany
christoph.hennersperger@tum.de

**Abstract.** We present a new system to acquire and reconstruct 3D freehand ultrasound volumes from arbitrary 2D image acquisitions over time. Motion artifacts are significantly reduced with a novel gating approach which correlates pulse oximetry data with Doppler ultrasound. The reconstruction problem is split into a ray-based sample selection on a per-scanline basis and a backward algorithm which is based on the concept of normalized convolution. We introduce an adaptive derivation of time-domain interpolation from the correlated pulse-oximetry and Doppler signals as well as an ellipsoid kernel size for spatial interpolation based on the physical resolution of the ultrasound data. We compare pulse-oximetry to classical ECG gating and further show the suitability of our normalized pulse signal for 3D+T reconstructions. The ease of use of the setup without the need of uncomfortable triggering via ECG provides the ability to use 3D+T ultrasound in every day clinical practice.

**Keywords:** freehand ultrasound, vascular, 4D, cardiac pulse phase, doppler, correlation, adaptive, reconstruction.

## 1 Introduction

Ultrasound imaging is an essential part of clinical imaging and plays a crucial role in diagnosis of cardiovascular diseases. Three dimensional (3D) ultrasound imaging is already used in obstetrics for diagnosis of facial abnormalities and has high potential for vascular imaging [4]. While 2D matrix array probes are providing 3D and 4D (3D+T) ultrasound information in realtime [10], they are - as conventional 1D array probes - limited in their field of view with respect to transducer design. Freehand ultrasound as an alternative or add-on technique allows the acquisition of high quality 3D ultrasound of steady anatomy; providing an extended field-of-view [11] and thus enables a better overview for physicians. For vascular applications though, the data is acquired over a certain period of time, in which the anatomy changes due to pulsating blood flow.

One major area where avoiding these artifacts is of crucial importance is 3D and 4D volume reconstruction (compounding). The goal here is to interpolate the acquired, irregulary sampled data onto a regular spatial 3D grid to enable an extraction of diagnostic indices (e.g. vessel volume from a segmentation) and visualization of the data in 3D. We propose the use of a fingertip pulse oximetry device,

D. Stoyanov et al. (Eds.): IPCAI 2014, LNCS 8498, pp. 68–77, 2014.

in addition to a 3D freehand ultrasound setup, recording B-Mode and Doppler ultrasound data, to reconstruct 3D volumes for desired cardiac pulse phases. This offers the possibility to accurately reconstruct pulse phase information while avoiding the cumbersome placement of electrodes for ECG gating, which is not applicable in many every-day screening applications with short investigation periods. Pulse oximeters are used as a standard tool in hospitals and allow the monitoring of the patient's oxygen saturation and heart frequency by analyzing the light absorption due to oxygenated red blood cells through thin tissue (i.e. finger or earlobe). However, as the sensors are measuring the local pulsation, which is not synchronous to cardiac excitation due to different patient anatomy, the signals cannot be used for interpolation without a reference to the ultrasound data.

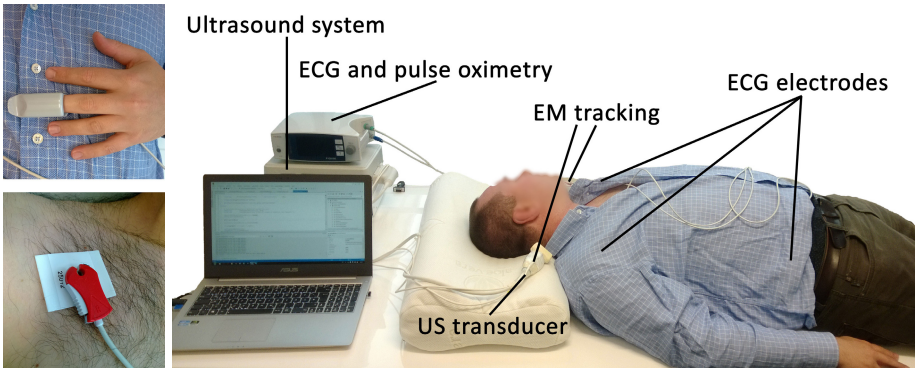


**Fig. 1.** The experimental setup consists of a combined pulse oximetry / ECG device, an open-access ultrasound system and two electomagnetic trackers mounted on the ultrasound probe. For ECG gating, three electrodes (left bottom) have to be mounted on three torso positions to retrieve a ECG curve, while for pulse-oximetry (left top), only a fingertip is required.

To provide high-quality reconstructions and make full use of the discussed system setup we propose a novel approach to correlate pulse oximetry with Doppler ultrasound information. This allows an automatic and accurate calibration of the pulse oximetry sensor individually for every acquisition. Thus, the pulse oximetry data can be used as a reference for constructing normalized pulse phase signals. The reconstruction of 3D+T volume data from single ultrasound scanlines is computed using a concept similar to normalized convolution [8] for $0-th$ order interpolation. We propose the selection of samples for the reconstruction of every voxel based on an ellipsoid region defined by the US properties around every sample in a backward transformation step. Therefore, we are able to split the sample-selection from the voxel interpolation to reconstruct smooth volumes with respect to the local spatial resolution of the original ultrasound sample data. We compare pulse-oximetry to ECG gating and further demonstrate the advantages of using adaptive time-domain interpolation for the application of carotid artery freehand ultrasound.

## 2 Related Work

Although ECG can be used to accurately detect cardiac phases for freehand ultrasound [2], the equipment needed is relatively cumbersome and consequently several alternative methods were developed relying on the ultrasound data only. First approaches based on filtering of intermediate signals containing cardiac information calculated from intensity values [13] or via the centroid algorithm [6] demonstrated good performances but needed either user input or were limited to certain areas. Further approaches based on phase correlation [12] and manifold learning with Laplacian eigenmaps [14] were successfully applied to US data for detection of both cardiac and respiratory motion. However, most of the proposed image-based methods rely on a constant pulse frequency for detection [13, 6, 12] and provide rough estimates of cardiac pulse phases [13, 6, 12, 14] which could introduce artifacts in 4D reconstruction with time-domain interpolation.

3D volume reconstruction methods can be grouped into pixel-based methods, voxel-based methods and function-based methods [11]. Pixel-based methods transform pixel values with a forward transformation into corresponding voxels. Voxel-based methods traverse every voxel and map back corresponding pixel values. Function-based methods estimate an interpolation function from the input data and evaluate the function at a regular grid. Recent advances in reconstruction methods also led to improvements by modeling US statistics in a physical way by using Nakagami distributions [7]. Although these methods provide volumetric data of exceptional quality, the computational demands prevent their application in time-critical applications. In [1] a similar reconstruction approach is used to carry out interpolation in the spatio-temporal (4D) domain. However they apply interpolation only in forward direction and do not consider adaptive interpolation in both spatial and temporal domain.

## 3 Methods

Our goal is to obtain an instensity value $I(v_i, \phi)$ for every voxel $v_i \in V$ in the Cartesian equidistant volume $V \in \mathbb{R}^3$ for a given timepoint $\phi$ in the cardiac pulse phase. We separate the ultrasound sample selection in spatial and temporal domain from the actual voxel reconstruction, as a sample selection in voxel coordinates (i.e. searching for the k nearest neighbours in the 4D volume) would ignore the physical and temporal information of our acquisition. Instead, we supply temporal and spatial weights for every sample-voxel relation to the reconstruction step. These weights are defined based on either the (temporal) pulse phase information, or the (spatial) ultrasound beam information. Therefore, the reconstruction approach is split into three parts: i) the retrieval of a normalized pulse phase signal for every acquisition; ii) a physics-based selection of ultrasound samples contributing to each voxel; and iii) the reconstruction of the final voxel intensity value from the selected samples.

### 3.1 Retrieval of Normalized Pulse Signal

We aim to reconstruct 4D data for different points within the cardiac pulse phase and thus introduce a fingertip pulse oximetry device as a reference sensor in the setup, which provides a measure of the oxygen saturation throughout the cardiac pulse phase. As pulse oximetry values are influenced by the percentage of blood that is loaded with oxygen [3], the measured signal changes during cardiac pulse phases and is related to changes in vessel diameter caused by volume-deviations. This is exactly what we are aiming for as changes in vessel diameter are the cause of "pulsatile" artifacts in ultrasound acquisitions. Consequently, the pulse-oximetry signal can not only be used for gating, as it is currently also done with ECG, but also to reconstruct a normalized pulse shape signal. This shape signal can then be used directly within the reconstruction.

In order to be able to utilize the pulse oximetry signal, we first have to carry out a calibration to the ultrasound data, as due to different anatomy and pulse-wave-velocities, the temporal offset between fingertip and target ultrasound location will vary among different acquisitions. For vascular applications, a second signal containing pulse phase information can be retrieved from the Doppler ultrasound components belonging to non-stationary, moving scatterers within the volume of interest. These components can be identified as the sum of all non-zero Doppler data components after clutter filtering of the ultrasound ensemble, where stationary and slowly moving components are removed from the signal. By having two signals containing pulse information, we can automatically map US data to cardiac pulse phases for individual acquisitions without any preconditions of a constant pulse frequency or the absence of arrhythmia. To enable a direct correlation, we extract an arterial flow velocity signal - corresponding to Doppler signals - from the pulse oximetry data by taking the gradient of the signal [3] (see Fig. 2a). Consequently, the time offset $o_{d\to p}$ between the corresponding data can be retrieved by finding the maximum cross-correlation of both real signals as:

$$o_{d\to p} = \arg\max_{l} \sum_{k=0}^{K-l-1} d_{k+l} * p'_k \quad w.r.t. \quad p'_k = \frac{\partial p_k}{\partial k}, \tag{1}$$

with $p'_k$ and $d_{k+l}$ representing the pulse derivative and shifted Doppler data with offset $l$ respectively. Based on the calibration, we can use the pulse-oximetry signal to reconstruct a normalized pulse shape signal $\bar{p}$. Therefore, we first automatically detect the set of $M$ pulse periods $[m_1, \ldots, m_M]$ in the pulse oximetry signal corresponding to the sets of pulse samples $p^m_{i\to j} = [p_i; p_j]$ as follows. As the distance $j - i$ between the peaks varies even within one acquisition, we use the average peak-to-peak distance $D = mean(j - i) \quad \forall i, j$ with $0 \leq i < j \leq K$ to map all pulse periods $p_{i\to j}$ to the same interval

$$\overline{p^m_{i\to j}} = p_i \ldots p_j \to p_1 \ldots p_D. \tag{2}$$

To preserve the shape of every pulse signal in an optimal way, we use cubic spline interpolation to conduct this mapping to the normalized pulse shapes.

To reconstruct a normalized pulse shape $\hat{p}$ from $m = 1 \dots M-1$ pulse periods $\overline{p_{i\to j}}$, we use a weighted average of all normalized pulse shapes, where the weight is defined by the deviation of the original shape period length to the average peak-to-peak distance

$$\hat{p} = \frac{1}{\Omega} \sum_{\forall m \in M} w_m \cdot \overline{p^m_{i\to j}} \tag{3}$$

$$w_m = 1 - \frac{|D - (j-i)|}{D}, \quad \Omega = \sum_{\forall m \in M} w_m. \tag{4}$$

The normalized pulse phase signal $\overline{p}$ can then be retrieved by mapping $\hat{p}$ to every peak-to-peak interval of $M$ accordingly by spline-interpolation. Figure 2b shows an example for resulting normalized pulse phases from given input data.

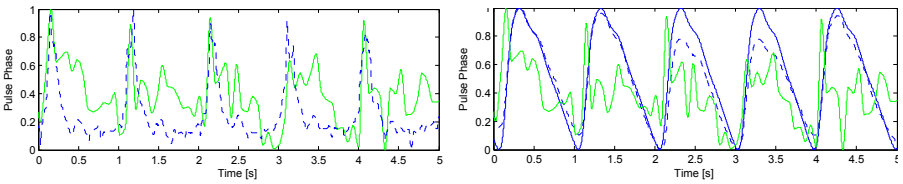


(a) Signal Calibration (b) Normalized Pulse Signal

**Fig. 2.** Left: arterial flow signal extracted from pulse oximetry (blue, dashed) used for time calibration with the Doppler signal (green, solid). Right: normalized pulse phase $\overline{p}$ (blue, solid) retrieved from Doppler data (green solid) and pulse oximetry (blue, dashed) for a freehand scan of the carotid artery.

### 3.2 Ultrasound Sample Selection

Before reconstructing a final intensity value, we have to select and weight contributing samples for every voxel based on spatial and temporal constraints. Every sample has a position $s_j$, normalized pulse value $\bar{p_j}$ and an intensity value $I(s_j)$. We first select samples for every voxel based on the voxel position in the sample coordinates. To do so, we set an ellispoid around every sample, representing its corresponding influence region

$$G_s(v_i, s_j) = \begin{cases} K(v_i, s_j) & \text{if } \frac{\left(v^{s_j}_{i,x} - s_{j,x}\right)^2}{d^2_{mx}} + \frac{\left(v^{s_j}_{i,y} - s_{j,y}\right)^2}{d^2_{my}} + \frac{\left(v^{s_j}_{i,z} - s_{j,z}\right)^2}{d^2_{mz}} \leq 1 \\ 0 & \text{otherwise,} \end{cases} \tag{5}$$

where $s_j$ is the position of sample $j$ in volume coordinates and $v_i^{s_j}$ the $i$-th voxel position in coordinates of sample $j$. The maximum spatial distances $d_{mx}, d_{my}, d_{mz}$ to the sample location are set according to the axial, lateral and

elevational resolution of the ultrasound data, defined by the transducer and acquisition properties [9] given by our US system (see Sec 3.4). We define the spatial weight of every US sample with respect to a target voxel based on the voxel position in relation to a three-dimensional exponential decay centered at the sample position $s_{j,x}, s_{j,y}, s_{j,z}$ of the current scanline ray sample $j$

$$K(v_i, s_j) = \frac{1}{(2\pi)^{\frac{3}{2}}|B|^{\frac{1}{2}}} e^{-\frac{1}{2}(v_i^{s_j} - s_j)^T B^{-1}(v_i^{s_j} - s_j)}, \quad B = diag(\sigma_x^2, \sigma_y^2, \sigma_z^2). \tag{6}$$

The spatial variances are set to $\sigma_x = \frac{1}{2}d_{mx}, \sigma_y = \frac{1}{2}d_{my}, \sigma_z = \frac{1}{2}d_{mz}$ to assure the ellipsoid cut-off at $2\sigma$ (95.4%). By specifying these distances based on the physical properties, only samples fullfilling these prior information are contributing to the final voxel intensity.

For the temporal selection of samples, weights are retrieved from a linear decay, according to the distance of the normalized pulse phase sample point $0 \leq \phi \leq 1$ to the desired reconstruction point $\phi$ with

$$G_t(\overline{p_j}, \phi) = \begin{cases} 1 - \frac{|\overline{p_j} - \phi|}{d_{mt}} & \text{if } |\overline{p_j} - \phi| \leq d_{mt} \\ 0 & \text{otherwise} \end{cases}, \tag{7}$$

which enables a reconstruction for any pulse point $\phi$ throughout the cardiac pulse phase.

### 3.3 Normalized Backward Reconstruction

In order to obtain the final intensity value $I(v_i, \phi)$ from our (sparse) set of samples, we make use of the concept of normalized convolution. Therefore, we modifiy the orginal concept [8] and apply it as a backward-transformation. By doing so, we can incorporate our spatial and temporal weights directly, while for a forward normalized convoluation, the weights would be retrieved from the convolution of the sample space with a fixed kernel, which would be unrelated to the ultrasound physics. We calculate the cumulative intensities $I_{cum}(v_i, \phi)$ and certainties $C_{cum}(v_i, \phi)$ by traversing all input samples $S = \{s_1, \ldots, s_j, \ldots, s_N\}, s_j \in \mathbb{R}^3$ for every voxel as

$$C_{cum}(v_i, \phi) = \sum_{\forall j \in S} G_s(v_i, s_j) \cdot G_t(\overline{p_j}, \phi) \cdot C(s_j) \tag{8}$$

$$I_{cum}(v_i, \phi) = \sum_{\forall j \in S} G_s(v_i, s_j) \cdot G_t(\overline{p_j}, \phi) \cdot I(s_j) \cdot C(s_j). \tag{9}$$

Here, $C(s_j) \in [0 \ldots 1]$ is a given certainty value for every input sample $s_j$, representing the reliability of the underlying data sample and $G_s$ and $G_t$ are the spatial and temporal weighting functions. Once all voxels have been traversed, $C_{cum}(v_i, \phi)$ states the total certainty of the individual voxels. It is noteworthy that $|G_s(v_i, s_j)| \leq \frac{1}{(2\pi)^{3/2}\sigma_x\sigma_y\sigma_z}$ for a single sample contributing to the surrounding voxels, thus $C_{cum}(v_i, \phi)$ is not limited to a specific value range. Consequently, the final volume intensity values can be reconstructed as:

$$I(v_i, \phi) = \frac{I_{cum}(v_i, \phi)}{C_{cum}(v_i, \phi)}. \tag{10}$$

### 3.4 Experimental Setup Protocol

All experiments in this work were carried out with an open access ultrasound system (Aurotech ultrasound AS, model MANUS) with a linear array probe (128 elements - single element width $0.27mm$, height $4mm$, focal depth $30mm$, 45 aperture elements) operating at 8MHz. For every dataset, pulse-oximetry as well as ECG data was acquired synchroneously with a combined POX-ECG system (Medlab GmbH, model P-OX100). An overview of the whole system is shown in Fig. 1.

***ECG Cross-Validation:*** As ECG gating still is mostly considered as the only alternative to achieve an accurate pulse gating, we validated our calibrated pulse-oximetry signals versus ECG slopes. For 6 subjects, 2 records each were acquired. As the total blood volume in the fingertip is influenced by the relative position of the finger w.r.t. the heart, signals could change for varying positions. In our experimental setup the overall patient position (lying on table, similar to conventional ultrasound examinations) was kept constant throughout the experiments, but the position of the fingertip changed for the two recordings to analyze POX signal changes. For the first records, the fingertip was placed at a relaxed position at the table, while for the second recordings the patients had to lift their fingers as high as possible. Scans of about $10s$ were acquired for each position. Subsequently, automatic pulse-oximetry to ultrasound calibration was carried out and additionally, a vessel-tracking method based on [5] employed to the ultrasound data to extract a vessel lumen diameter signal from the recorded 2D frames as an index of vessel expansion and compression. For validation, the pulse peaks were extracted manually from the ECG, the lumen diameter and our normalized pulse signals to compare the distances between the diameter signal and the ECG and POX signals respectively.

***Evaluation of Resolution-Preserving Reconstruction:*** Without time-domain interpolation, cardiac pulsation will either cause the appearance of a "pulsating" vessel in the 3D volume for low frame density or a loss of contour sharpness in regions where deformation is visible throughout the cardiac cycle. The consequence is that a potential diagnostic value would be falsified and the robustness and accuracy of image processing methods affected in general. Thus we evaluate the suitability of our novel normalized pulse phase signal for both cases and compare it to i) a constant volume without time-domain consideration; ii) a linear monotonic increasing pulse phase signal between subsequent pulse peaks, and iii) a linear pulse signal from mininmum to maximum peaks and vice versa. As before, scans of 6 volunteers were conducted, where for every subject both a slow (mean length $58.48s$) and a fast scan (mean length $22.32s$) of the carotid artery was acquired. For all datasets, volumes were reconstructed with a spacing of $0.25mm$ for the four compared methods. The maximum temporal distance $d_{mt}$ was decreased stepwise to $d_{mt} = [\frac{1}{2}, \ldots, \frac{1}{20}] = \frac{1}{2n_s}, n_s = 1 \ldots 10$, which is

equivalent to a subdivision of each cardiac pulse phase in $n_s$ steps. We compare how well the original US data is preserved in the reconstructed 3D volumes by evaluating the Mean Squared Error (MSE) of the reconstructed volumes $\in [0, 1]$ with respect to the input samples at their corresponding locations.

## 4 Results and Discussion

The results for the POX-ECG validation of all compared distances are shown in Table 1. It can be seen that i) the peak to peak distance of the normalized pulse signal is almost identical to the ECG data (mean distance of 1.2ms), and ii) the calibrated pulse signals have a mean deviation to the extracted diameter signal of $-34ms$. As the temporal resolution of the diameter signal extracted from the ultrasound data is low compared to the other signals (12Hz compared to 100Hz for POX and ECG signals), a standard deviation approximately equal to the ultrasound sampling period (83.3ms) is considered as optimal, which is facilitated by the standard deviation of the peak-to-peak distances in the vessel diameter signal (104.9ms). As the deviation of the normalized pulse peaks is perfectly within this range, the extracted ultrasound signal is the limiting factor to the general accuracy. This suggests that the pulse oximetry signal is well-suited for gating of ultrasound acquisitions.

**Table 1.** Signal pulse period results. Shown are the peak distances between the pulse oximetry and ECG signal, as well as the distance from the pulse oximetry and ECG signals respectively to the vessel diameter signal.

| Distance Comparison | Finger Position | | | |
|---|---|---|---|---|
| | Relaxed | | Lifted | |
| | $\mu[s]$ | $\sigma[s]$ | $\mu[s]$ | $\sigma[s]$ |
| $\Delta$ Area | - | 0.1049 | - | 0.1023 |
| $\Delta$ $\overline{p}$ to ECG | 0.0009 | 0.0187 | 0.0016 | 0.0229 |
| $\Delta$ $\overline{p}$ to Area | -0.0341 | 0.0774 | -0.0285 | 0.0799 |
| $\Delta$ ECG to Area | -0.2178 | 0.0858 | -0.1349 | 0.1348 |

Results for the evaluation fo the time interpolation scheme are shown in Fig. 3 for all methods. When comparing slow and fast ultrasound scans, it becomes clear that for the fast scans, the input ultrasound information is preserved best without time domain consideration. Disregard of the pulse information is still not recommendable, as this would potentially distort diagnostic values extracted from the volume datasets. For both slow and fast scans it can be observed that our normalized pulse phase provides the lowest errors for the different number of time steps and further preserves the input information better as a static reconstruction for slow scans. This preservation is visualized in Fig. 4, where a reconstruction without considering pulse information is compared to our method considering pulse information. For the former, edges are appearing less sharp and details get lost by using all input samples from different pulse phases for the reconstruction. With our method, details and edges are preserved much better.

Beyond that also a time-domain analysis is enabled by having distinct volume datasets for every point along the cardiac pulse phase.

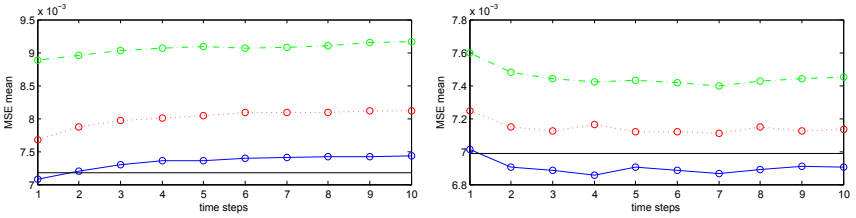


(a) Fast Scans (b) Slow Scans

**Fig. 3.** Reconstruction sample preservation. Shown is the mean MSE averaged over all fast/slow scans. The black solid line equals the baseline error without time-domain consideration. Compared is our method (blue, solid) to the linear pulse phase (red, dotted) and the min-to-max linear (green, dash-dotted).

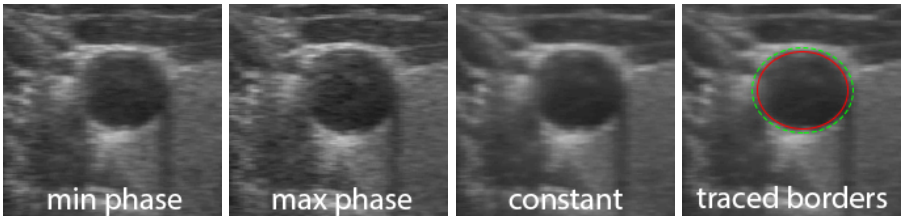


**Fig. 4.** Reconstruction for different pulse phases. Shown are cross-sectional slices through the vessel for min./max. vessel expansion, a volume without consideration of pulse data (constant) and overlaid contours for min./max. expansion.

***Setup Robustness:*** In respect of the presented experiments, we did not notice significant distortions of the pulse oximetry signals as long as the patients did not move their fingers during acquisition. However, as opposed to pulse oximetry, for placement of the ECG electrodes, full attention was necessary in all experiments to provide useful signals. Thus we suggest that especially for time-critical situations, our technique could be a promising and robust alternative to classical gating. However to confirm these assumptions w.r.t to a direct clinical application, a thorough validation of the presented system is neccessary; especially in regard to different patient conditions (e.g. arrythmia or calloused finger skin) and working environments with possible distortions such as operating lights.

## 5 Conclusion

We presented a new system to reconstruct 3D+T volume data from freehand ultrasound in combination with a pulse oximetry sensor. We introduced a novel method for correlating pulse oximetry with Doppler ultrasound, enabling an accurate time-calibration on a per-record basis. We further showed how a normalized pulse phase signal can be defined based on the pulse oximetry data to

be used directly within time-domain interpolation. The setup can be used to reconstruct 3D volume data for cardiac pulse phases superior compared to today's freehand approaches and delievers improved capabilities for vascular ultrasound reconstruction compared to classical ECG gating. Furthermore, the uncomfortable use of ECG electrodes can be circumvented, which allows a more extensive use of 3D+T in every-day clinical scenarios.

## References

[1] Bosch, J., van Stralen, M., Voormolen, M., Krenning, B., Lancee, C., Reiber, J., van der Steen, A., De Jong, N.: Improved spatiotemporal voxel space interpolation for 3D echocardiography with irregular sampling and multibeat fusion. In: Ultrasonics Symposium, pp. 1232–1235. IEEE (2005)

[2] Brattain, L.J., Howe, R.D.: Real-time 4D ultrasound mosaicing and visualization. In: Proc. 14th Intern. Conf. Med. Image Comput. Comput. Assist. Interv., pp. 105–112 (2011)

[3] Cook, L.B.: Extracting arterial flow waveforms from pulse oximeter waveforms. Anaesthesia 56(6), 551–555 (2001)

[4] Forsberg, F.: Ultrasonic biomedical technology; marketing versus clinical reality. Ultrasonics 42, 17–27 (2004)

[5] Guerrero, J., Salcudean, S.E., McEwen, J.A., Masri, B.A., Nicolaou, S.: Real-time vessel segmentation and tracking for ultrasound imaging applications. IEEE Transactions on Medical Imaging 26(8), 1079–1090 (2007)

[6] Karadayi, K., Hayashi, T., Kim, Y.: Automatic image-based gating for 4D ultrasound. In: 28th Annual International Conference of the IEEE Engineering in Medicine and Biology Society, EMBS 2006, pp. 2388–2391 (2006)

[7] Klein, T., Hansson, M., Navab, N.: Modeling of multi-view 3D freehand radio frequency ultrasound. In: Ayache, N., Delingette, H., Golland, P., Mori, K. (eds.) MICCAI 2012, Part I. LNCS, vol. 7510, pp. 422–429. Springer, Heidelberg (2012)

[8] Knutsson, H., Westin, C.F.: Normalized and differential convolution. In: Proceedings of the 1993 IEEE Computer Society Conference on Computer Vision and Pattern Recognition, CVPR 1993, pp. 515–523 (1993)

[9] Ng, A., Swanevelder, J.: Resolution in ultrasound imaging. Continuing Education in Anaesthesia, Critical Care & Pain 11, 186–192 (2011)

[10] Prager, R., Ijaz, U., Gee, A., Treece, G.: Three-dimensional ultrasound imaging. In: Proc. Institution of Mechanical Engineers, Part H: Journal of Engineering in Medicine, vol. 224, pp. 193–223 (2010)

[11] Solberg, O.V., Lindseth, F., Torp, H., Blake, R.E., Nagelhus Hernes, T.A.: Freehand 3D ultrasound reconstruction algorithms - a review. Ultrasound in Medicine and Biology 33, 991–1009 (2007)

[12] Sundar, H., Khamene, A., Yatziv, L., Xu, C.: Automatic image-based cardiac and respiratory cycle synchronization and gating of image sequences. In: Yang, G.-Z., Hawkes, D., Rueckert, D., Noble, A., Taylor, C. (eds.) MICCAI 2009, Part II. LNCS, vol. 5762, pp. 381–388. Springer, Heidelberg (2009)

[13] Treece, G., Prager, R., Gee, A., Cash, C., Berman, L.: Grey-scale gating for freehand 3D ultrasound. In: Proceedings of the 2002 IEEE Intern. Symposium on Biomedical Imaging, pp. 993–996 (2002)

[14] Wachinger, C., Yigitsoy, M., Navab, N.: Manifold learning for image-based breathing gating with application to 4D ultrasound. In: Jiang, T., Navab, N., Pluim, J.P.W., Viergever, M.A. (eds.) MICCAI 2010, Part II. LNCS, vol. 6362, pp. 26–33. Springer, Heidelberg (2010)